

Review

# A Review of Mineral and Rock Wettability Changes Induced by Reaction: Implications for CO<sub>2</sub> Storage in Saline Reservoirs

Ting Chen <sup>1</sup>, Laiming Song <sup>2</sup>, Xueying Zhang <sup>3</sup>, Yawen Yang <sup>1</sup>, Huifang Fan <sup>1,\*</sup> and Bin Pan <sup>1,\*</sup>

<sup>1</sup> School of Civil and Resource Engineering, University of Science and Technology Beijing, No. 30, Xueyuan Road, Beijing 100083, China

<sup>2</sup> China National Offshore Oil Corporation Research Institute Co., Ltd., Beijing 100028, China

<sup>3</sup> PetroChina Huabei Oilfield Company, Renqiu 062552, China

\* Correspondence: fanhuifang@ustb.edu.cn (H.F.); binpan@ustb.edu.cn (B.P.)

**Abstract:** Wettability in CO<sub>2</sub>-brine-mineral/rock systems is an important parameter influencing CO<sub>2</sub> storage capacities and leakage risks in saline reservoirs. However, CO<sub>2</sub> tends to react with various minerals and rocks at subsurface conditions, thus causing temporal and spatial wettability changes. Although many relevant research works have been published during past years, a thorough overview of this area is still lacking. Therefore herein, reaction-induced wettability changes are reviewed, and the underlying mechanisms are discussed. Current research gaps are identified, future outlooks are suggested, and some conclusions are drawn. The fundamental understanding of reaction-induced mineral and rock wettability changes during CO<sub>2</sub> storage in saline reservoirs is analyzed and the guidance for long-term CO<sub>2</sub> containment security evaluations is provided.

**Keywords:** wettability; reactions; CO<sub>2</sub> storage in saline reservoirs; minerals; rocks



**Citation:** Chen, T.; Song, L.; Zhang, X.; Yang, Y.; Fan, H.; Pan, B. A Review of Mineral and Rock Wettability Changes Induced by Reaction: Implications for CO<sub>2</sub> Storage in Saline Reservoirs. *Energies* **2023**, *16*, 3484. <https://doi.org/10.3390/en16083484>

Academic Editor: Roland W Lewis

Received: 13 March 2023

Revised: 5 April 2023

Accepted: 12 April 2023

Published: 17 April 2023



**Copyright:** © 2023 by the authors. Licensee MDPI, Basel, Switzerland. This article is an open access article distributed under the terms and conditions of the Creative Commons Attribution (CC BY) license (<https://creativecommons.org/licenses/by/4.0/>).

## 1. Introduction

Carbon dioxide (CO<sub>2</sub>) storage in saline reservoirs is considered a promising technology to reduce carbon emissions and mitigate global warming [1–3]. In rock-aqueous fluid-nonaqueous fluid systems, the terms hydrophilic and hydrophobic represent the affinity of rocks to aqueous fluids [4]. Wettability affects many important parameters in the systems, such as residual non-aqueous fluid saturation [5,6], fluid morphology and interfacial region [6–9], relative permeability [6,10], and the relationship between capillary force and water phase saturation [6,7,11]. During the process of CO<sub>2</sub> storage in saline reservoirs, wettability directly affects structural and capillary trapping mechanisms [5–7,10–12], and indirectly affects dissolution and mineral trapping mechanisms by influencing the characteristics of the gas-liquid-rock interface [7,9,13]. This parameter is usually characterized by the brine contact angle ( $\theta$ ) in the CO<sub>2</sub>-brine-mineral/rock systems [4,14]. It is a complex function of rock/mineral properties, brine properties and thermo-physical conditions [4,11,15–21]. Throughout the entire lifetime of this storage, a series of reactions, acid-base reactions and mineral dissolution reactions [22–27] take place, which causes temporal/spatial changes in rock/mineral wettability and influences CO<sub>2</sub> storage capacities and containment securities [28–30]. Therefore, it is necessary to determine this parameter accurately under the consideration of the in-situ reactions.

Although some research works have been reported on rock/mineral wettability changes induced by reaction during the process of CO<sub>2</sub> storage in saline reservoirs, a review on this topic is still lacking. Some reviews have summarized the storage mechanism of CO<sub>2</sub>, changes in reservoir physical properties and physicochemical processes during storage. But they do not cover the wettability changes during physicochemical processes [31–33]. Therefore herein, this topic is systematically reviewed and current research gaps are clearly indicated. Future research directions are explicitly identified and some

conclusions are critically drawn. The fundamental understanding of reaction-induced mineral and rock wettability changes during CO<sub>2</sub> storage in saline reservoirs is analyzed and essential implications for long-term CO<sub>2</sub> containment security evaluations are provided.

## 2. Contact Angle Measurements

Contact angle ( $\theta$ ) measurement is the most direct and common method used to characterize the wettability of minerals/rocks [4,34].  $\theta$  are measured in two ways, the sessile drop method and the bubble capture method, as shown in Figure 1a. There are many types of contact angles [17], as shown in Figure 1b. The equilibrium contact angles include Young's contact angle ( $\theta_Y$ ) and the static contact angle ( $\theta_S$ ). The dynamic contact angle includes the advancing contact angle ( $\theta_A$ ) and the receding contact angle ( $\theta_R$ ).  $\theta_Y$  is only applicable to ideal solids with uniform, isotropic, smooth, and rigid surfaces [35]. The contact angle data summarized in this paper were measured using one of two methods, except for special instructions, as shown in Table A1.

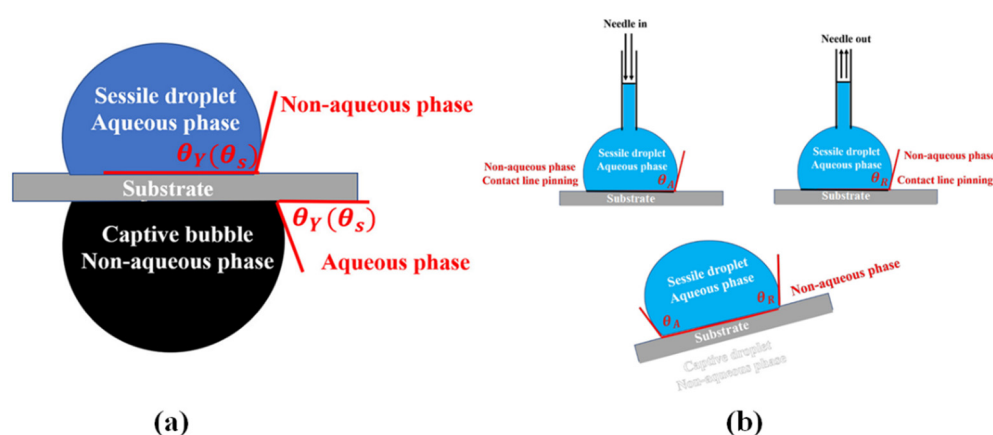


**Figure 1.** (a) Schematic diagram of methods for sessile drop and bubble capture; (b) Schematic diagram of dynamic contact angle measurement. (modified from [17]).

## 3. Reaction-Induced Wettability Changes in the CO<sub>2</sub>-Brine-Mineral Systems

Wettability changes are usually induced by reactions of CO<sub>2</sub> with the following minerals.

### 3.1. Quartz

Quartz is one of the most common minerals in a saline reservoir [4]. After exposure of quartz to water saturated CO<sub>2</sub> at 1.4 MPa~20.7 MPa and 25 °C for four cycles, the static water contact angle ( $\theta_S$ ) in the CO<sub>2</sub>-water-quartz system increased from 40°~50° to 80°~90°, respectively [36], as shown in Figure 2. One cycle consists of a pressure increasing stage from 1.4 MPa to 20.7 MPa and a decreasing stage from 20.7 MPa to 1.4 MPa. This observation is qualitatively consistent with that in another report [37]. After supercritical CO<sub>2</sub> (scCO<sub>2</sub>) displaced NaCl brine with various salinities (0.01 M, 1 M, 3 M, 5 M) in a silica micromodel for 20 min at 8.5 MPa and 45 °C, the brine droplets gradually formed and the average  $\theta_S$  increased from 0° to 54°, 66°, 65°, 75° correspondingly [37], as shown in Figure 3. In this process, brine was pumped out at a rate of 4  $\mu$ L/min and scCO<sub>2</sub> was injected in at constant pressure. In contrast, after CO<sub>2</sub>, 0.171 M NaCl brine and quartz contacted overnight at various temperatures (38 °C and 55 °C) and pressures (6 MPa~12.1 MPa),  $\theta_S$  varied within the range of 21°~25°. This phenomenon shows  $\theta_S$  is irrelevant of temperature and pressure at this condition [38]. It also indicates that quartz wettability still remains strongly water-wet in this situation [39], as shown in Figure 2.

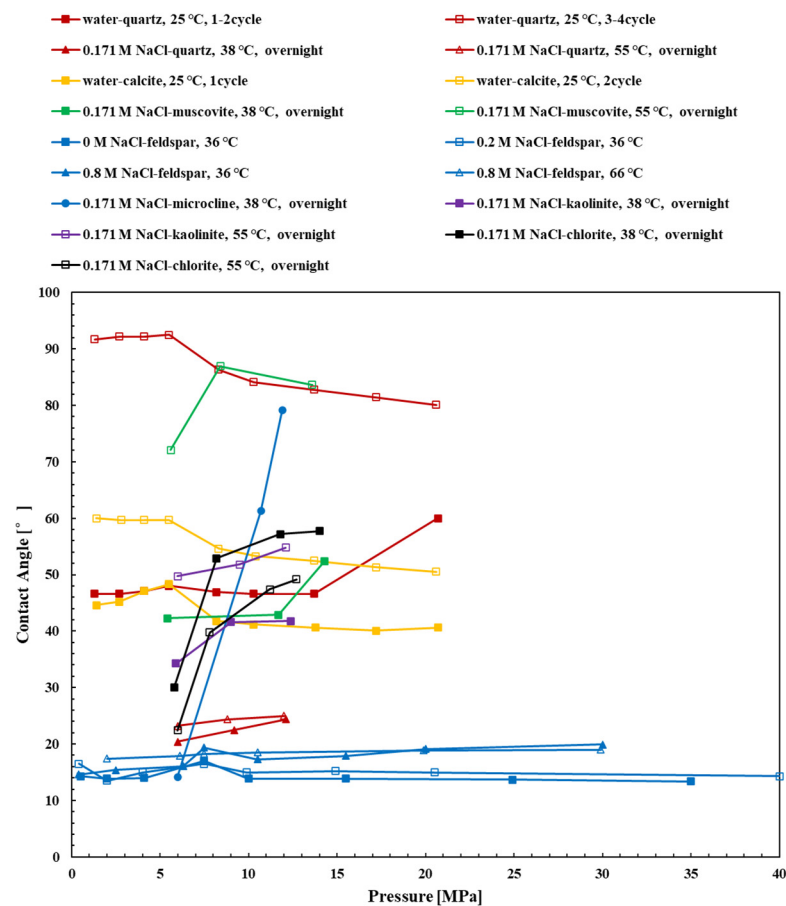


**Figure 2.** Water contact angle as a function of pressure, temperature and salinity in the CO<sub>2</sub>-NaCl brine-mineral systems after minerals reacted with CO<sub>2</sub> for various periods [36,38,40]. Pressure increased from 1.4 MPa to 20.7 MPa and then decreased to 1.4 MPa again as 1 cycle [36].

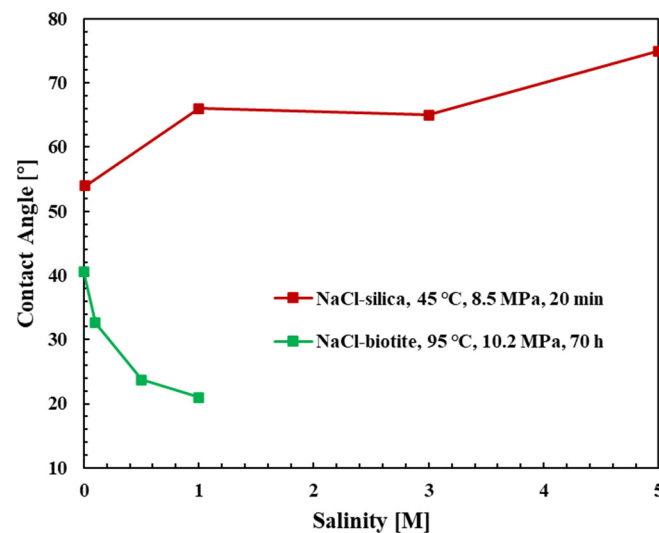


**Figure 3.** Water contact angle as a function of salinity in the CO<sub>2</sub>-NaCl brine-mineral systems after reaction with CO<sub>2</sub> for different periods [37,41].

Initially the pores are filled with brine, as shown in Figure 4a. After the injection of scCO<sub>2</sub>, the residual brine covers the silica surface to form a water film due to the hydrophilic nature of the silica, as shown in Figure 4b. However, CO<sub>2</sub>-brine-quartz reaction can make the water film thinner and lead to the formation of isolated brine droplets and

gas bubbles on the silica surface, as shown in Figure 4c. These results clearly indicate that the contact angle of brine increases, and the hydrophilicity of the silica surface is weakened. The underlying mechanism for this phenomenon can be attributed as follows: (1) the dissolution of  $\text{CO}_2$  decreases the pH; (2) the dissociated  $\text{H}^+$  adsorbs the negative silica surface; (3) The surface charge density decreasing causes the water film to become thinner [42].

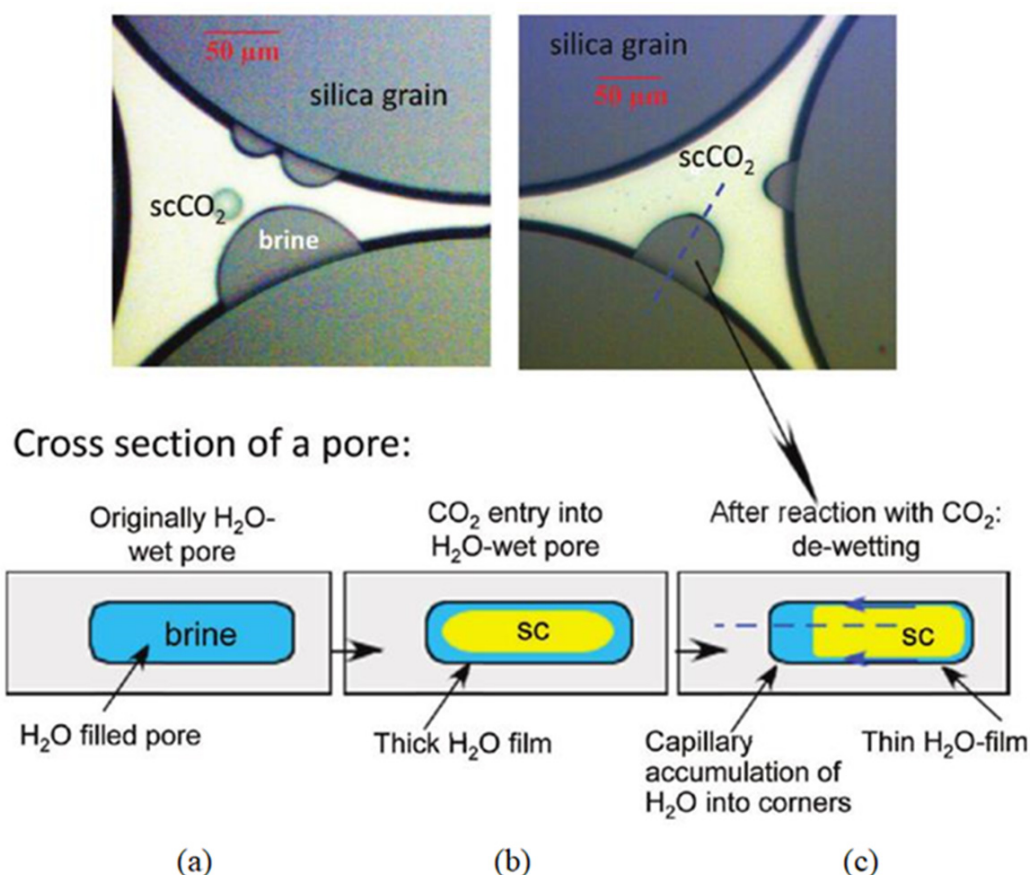


**Figure 4.** Schematic of water film thinning process due to  $\text{CO}_2$  injection in porous media [37]. (a) brine filled pore; (b)  $\text{CO}_2$  entry into pore; (c) reaction induced water film thinner. (Reprinted with permission from [37]. Copyright 2012 American Chemical Society).

### 3.2. Calcite

Calcite is the dominant mineral in carbonate reservoirs and tends to react with  $\text{CO}_2$  and brine at subsurface conditions. These reactions cause possible changes in wettability [43].

During the process of  $\text{CO}_2$ -0.8 M NaCl brine-calcite reactions at 10.5 MPa and 36 °C,  $\theta_5$  increased from 10° to 13° in the first 4 days and then remained stable for a longer time [40], as shown in Figure 5. In contrast, after calcite was exposed to water saturated  $\text{CO}_2$  at 1.4 MPa and 20.7 °C for two cycles,  $\theta_5$  increased about 10°~20° (from 40°~50° to 50°~60°) in the water saturated  $\text{CO}_2$ - $\text{CO}_2$  saturated water-calcite system [36], as shown in Figure 2. In another work,  $\theta_5$  was measured as a function of pressure, temperature, pH and reaction time in the  $\text{CO}_2$ -water-calcite system [44]. The results demonstrated that (1)  $\theta_5$  slightly increased from 21° to 24° with increasing pH from 3 to 5.9 at 30 °C and 7 Mpa due to the surface charge reduction; (2)  $\theta_5$  increased significantly from 25° to 47° due to stronger  $\text{CO}_2$  mass transfer and smaller pH = 3 at 50 °C and 20 Mpa. (The pH value of the same brine at room temperature and pressure is 7.8.); and (3) after calcite reacted with  $\text{CO}_2$  for a long time (3 weeks),  $\theta_5$  did not change clearly, though calcite had a loss in mass.

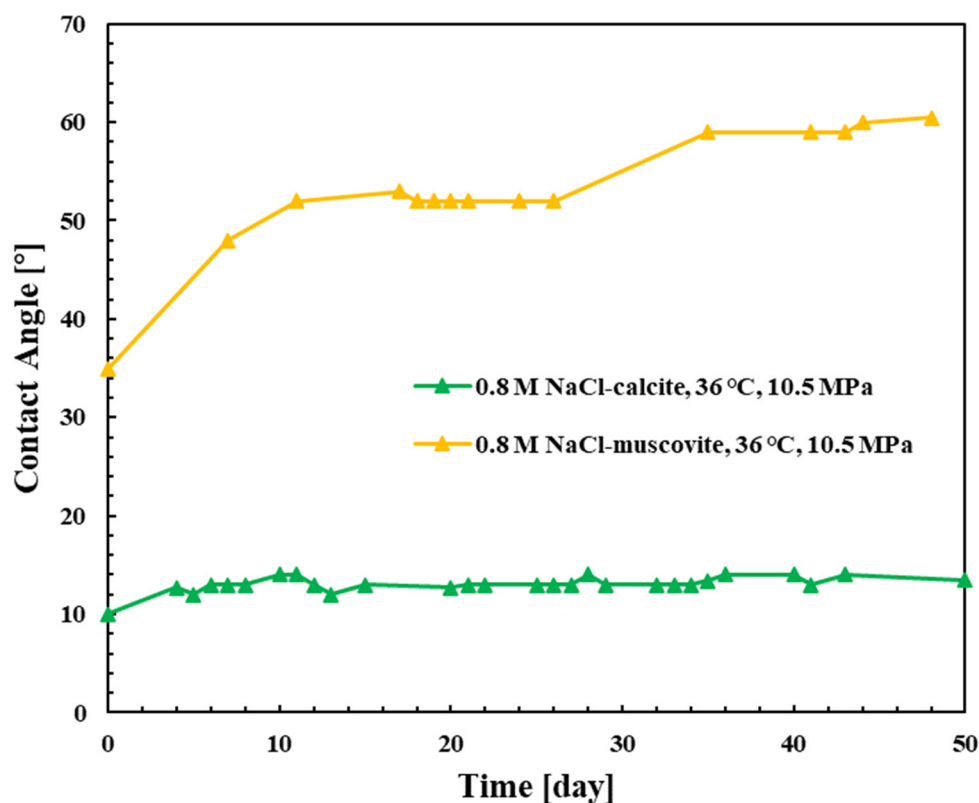


**Figure 5.** Water contact angle as a function of reaction duration in the CO<sub>2</sub>-NaCl brine-mineral systems after reaction with CO<sub>2</sub> [40].

The underlying mechanism for the observed increase in  $\theta_S$  is attributed as follows: (1) CO<sub>2</sub> induced chemical reactions promote a weak carbonic acid formation, as shown in Equations (1)–(3) [45]; (2) Calcite dissolves and its surface heterogeneity increases [46]; and (3) The hydrophilicity of calcite decreases [36,40]. The possible reason for the plateaued  $\theta_S$  at late stages is that the surface charges on calcite surfaces are invariable because reactions at this moment are relatively weak [40].



### 3.3. Mica

Mica is one of the dominant minerals in caprocks and thus its wettability determines the structural CO<sub>2</sub> storage capacities and containment securities [21,42].

After muscovite reacted with CO<sub>2</sub> and 0.8 M NaCl brine at 36 °C and 10.5 MPa for 48 days,  $\theta_S$  increased from 35° to 60° [40], as shown in Figure 5. This observation is qualitatively consistent with another report [38]. After muscovite reacted with CO<sub>2</sub>-0.171 M NaCl brine at various temperatures (38 °C and 55 °C) and pressures (5.4 MPa~14.3 MPa) overnight,  $\theta_S$  increased with temperature and pressure. For example,  $\theta_S$  increased from 42° to 72° with the temperature increase from 38 °C to 55 °C at 5.5 MPa. Then  $\theta_S$  increased from 72° to 82° with the pressure increase from 5.5 MPa to 13.6 MPa at 55 °C, as shown in Figure 2. In principle, CO<sub>2</sub> induced chemical reactions promote a weak carbonic acid formation, as shown in Equation (1). Then H<sup>+</sup> from the solution is adsorbed onto the negatively charged mica surface. The surface charge density on the mica surface are

reduced. As a result, the electrostatic interaction (repulsive) forces, which used to stabilize the water film, are decreased.  $\theta_S$  increased with reaction time [40]. Another underlying mechanism for the wettability alteration is possibly due to the swell and delamination off of the muscovite [38].

There are some reports on the impact of reactions on biotite wettability at in-situ CO<sub>2</sub> storage conditions. After biotite reacted with NaCl brine at various salinities (DI water, 0.1 M, 0.5 M, and 1 M NaCl) at constant thermo-physical conditions (95 °C and 10.2 MPa) for 70 h,  $\theta_S$  decreased from 41° to 21° which was measured at 10.2 MPa and 48 °C [41], as shown in Figure 3. Fundamentally, salinity induced chemical reactions promoted biotite dissolution and ion exchange. As a result, biotite surface structure, compositions and potential were changed. For example, when NaCl salinity increased from 0 M to 1 M, surface roughness increased from 1.5 nm to 16.6 nm and hydroxyl content increased from 82.9% to 92.9% while zeta potential decreased from −19 mV to −47.6 mV, as shown in Table 1. However, the type of chemical reactions exactly occurred during this process were not specified in this work.

**Table 1.** Surface properties of biotite after biotite reacted with CO<sub>2</sub> for 70 h under different salinity conditions (modified from [41]).

Salinity	Static Contact Angle [°]	Surface Roughness [Rq, nm]	Zeta Potential [mV]	Surface Hydroxyl Content [%]
DI water	41 ± 3	1.5 ± 0.2	−19.1	82.9
0.1 M NaCl	33 ± 1	2.9 ± 0.7		
0.5M NaCl	24 ± 2	5.6 ± 0.2		
1.0M NaCl	21 ± 2	16.6 ± 1.3	−47.6	92.9

Phosphate, sulfate, phosphate (DTPMP), oxalate and acetate were dissolved in 1M NaCl solution to individually form different aqueous solutions [47–50]. After biotite reacted with CO<sub>2</sub> and different solutions at 95 °C and 10.2 MPa for 96 h,  $\theta_S$  changed by different degrees. For example,  $\theta_S$  decreased by 7°~17° after the first four reactions. The reason for the enhanced wettability was that the hydrophilic functional groups on the biotite surface were exposed and more negative charges were generated at the fracture edges due to the adsorption of the above water chemicals.  $\theta_S$  for biotite increased by 17°, increasing from 27° to 44°, after the last reaction. Acetate adsorption made the surface hydroxyl group of biotite inward, and the hydrophobic methyl group was exposed on the surface, thus weakening the wettability.

### 3.4. Feldspar and Microcline

For the CO<sub>2</sub>-NaCl brine-feldspar system,  $\theta_S$  was almost a constant in the range of 10°~20° with no significant change at various pressures (0 MPa~40 MPa), temperatures (36 °C and 66 °C) and NaCl salinities (0.2 M and 0.8 M), as shown in Figure 2. Fundamentally, the feldspar surface charges are positive and the reactions with H<sup>+</sup> are not significant in the range of pH (3~5) [40]. In contrast, the contact angle decreased from 23° to 18° with increasing pH from 3 to 5.9 at 30 °C and 7 MPa due to the increase of surface charge [44]. Furthermore, after microcline reacted with CO<sub>2</sub>-0.171 M NaCl brine at 38 °C overnight,  $\theta_S$  increased from 95° to 125° when the pressure increased from 5.5 MPa to 13.8 MPa [38], as shown in Figure 2.  $\theta_S$  was measured at reaction conditions. These results were not consistent with the hydrophilicity of feldspar above and the underlying mechanism is possibly due to the microcline heterogeneity caused by K (kalium) deficiency. However, further experiments are required to verify this hypothesis.

### 3.5. Kaolinite and Illite

After kaolinite reacted with CO<sub>2</sub>-0.171 M NaCl brine at various temperatures (38 °C; 55 °C) and pressures (5.9 MPa~12.4 MPa) overnight,  $\theta_S$  increased with temperature and was

insensitive to pressure [38]. For example,  $\theta_S$  increased from 34° to 50° with the temperature increase from 38 °C to 55 °C at 6 MPa.  $\theta_S$  increased from 50° to 55° with the pressure increase from 6 MPa to 12.1 MPa at 55 °C, as shown in Figure 2. This is because CO<sub>2</sub>-brine induced chemical reactions, Equations (1)–(4) [38], promoted kaolinite dissolution and changed concentrations of kaolinite surface elements, such as Fe, Ca, K.



On the other hand, one report [44] argued that the CO<sub>2</sub> induced reaction involves surface ion exchange between clays (e.g., kaolinite and illite) and brine [51]. In addition, dissolution and precipitation also affect the electrical double layer and thus change the  $\theta_S$  of kaolinite and illite [52].

### 3.6. Chlorite

So far there is only one report on the influence of reactions on chlorite wettability at in-situ CO<sub>2</sub> storage conditions [38]. After chlorite reacted with CO<sub>2</sub>-0.171 M NaCl brine at various temperatures (38 °C and 55 °C) and pressures (5.8 MPa~14 MPa) overnight,  $\theta_S$  increased with pressure but decreased with temperature. For example,  $\theta_S$  increased from 30° to 58° with the pressure increase from 5.8 MPa to 14 MPa at 38 °C. Contrary to this,  $\theta_S$  decreased from 30° to 22° with the temperature increase from 38 °C to 55 °C at 6 MPa, as shown in Figure 2. The underlying mechanisms for the weakened wettability are attributed to chemical reactions between chlorite and CO<sub>2</sub>-brine, promoting chlorite dissolution. The chlorite surface structure is changed and wettability of chlorite is decreased. However, no quantitative information was provided on the chlorite surface roughness in this work. On the other hand,  $\theta_S$  decreased with the increase of reaction temperature. This phenomenon is different from that of other minerals, such as quartz, mica and kaolinite. This might be due to the inhibition of the above reactions or the occurrence of new reactions at higher temperature (55 °C vs 38 °C). However,, these assumptions have not been verified.

## 4. Reaction-Induced Wettability Changes in the CO<sub>2</sub>-Brine-Rock Systems

Wettability changes are usually induced by reactions of CO<sub>2</sub> with the following rocks.

### 4.1. Shale

Shale is the main caprock rock used for CO<sub>2</sub> storage in saline reservoir and its features are closely related to the storage capacities and leakage risks of CO<sub>2</sub> [11,53].

Three shale samples, LM 1, LM 2 and YC, were collected from Longmaxi formation and Yanchang formation. After shale samples reacted with CO<sub>2</sub> for 12 days at 40 °C and 8 MPa, their  $\theta_S$  increased from 57° to 70°, from 57° to 70°, and from 61° to 85°, respectively, which were measured at 0.1 MPa and 25 °C [13,54], as shown in Figure 6.

Three shale samples, WF, EF and MAN, were collected from Wolfcamp, Eagle Ford and Mancos formations, respectively. After shale samples reacted with scCO<sub>2</sub> at 70 °C, 18 MPa for 30 days, it was found that  $\theta_S$  of WF increased from 71° to 90° and  $\theta_S$  of EF increased from 65° to 100° while  $\theta_S$  of MAN decreased from 36° to 25°, measured at 0.1 MPa and 20 °C [29,55], as shown in Figure 6. Five shale samples were collected from an outcrop in Labuan (L 1, L 2, L 3, L 4 and L 5). After shale samples reacted with scCO<sub>2</sub> for 6 months at 17.9 MPa and 50 °C, the advancing contact angle ( $\theta_A$ ) increased from 39°~46° to 43°~57° in the system of CO<sub>2</sub>-shale-deionized water which were measured at 15 MPa and 50 °C [28], as shown in Figure 6. However, no brine participation occurred in the reaction period. The conclusion in this work that low salinity is beneficial to stabilize shale wettability needs to be further verified.

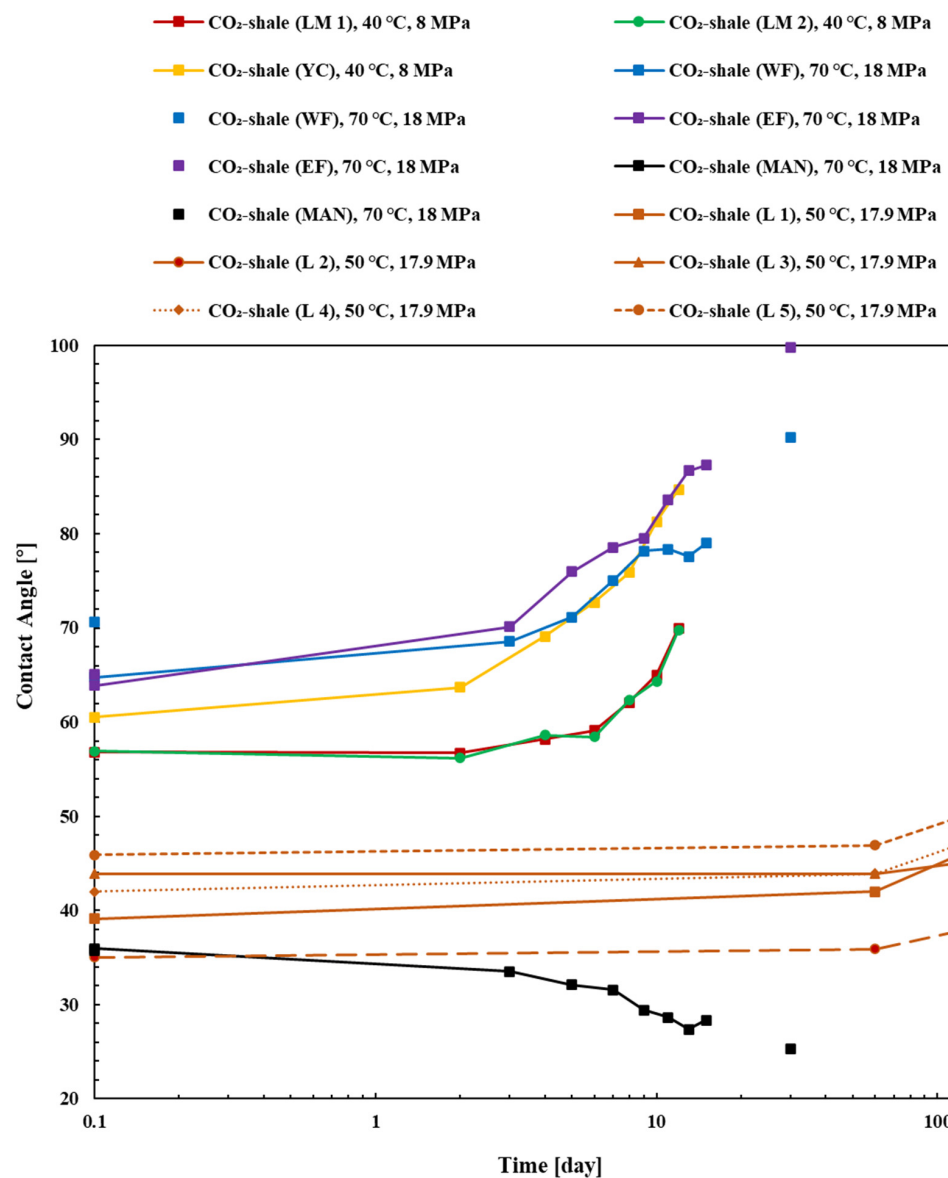


**Figure 6.** Water contact angle as a function of reaction duration in the H<sub>2</sub>O-rock systems after reaction with CO<sub>2</sub> [13,28,29,54,55]. The contact angle for conditions of 50 °C and 17.9 MPa are advancing; as is the contact angle measured at 50 °C and 15 MPa [28]. To facilitate data analysis, the starting point 0 was approximated to 0.1.

Meanwhile, the wettability is also a function of the reaction pressure. After shale samples reacted with CO<sub>2</sub> at various pressures (6 MPa, 8 MPa, 10 MPa, 12 MPa, 14 MPa, 16 MPa and 18 MPa) at 40 °C for 12 days,  $\theta_s$  for shales (LM 1, LM 2 and YC) increased from 62° to 89° and from 64° to 90°, respectively, which were measured at 0.1 MPa and 25 °C [13,54], as shown in Figure 7. Pressure changes with two days interval. Shale sample (LM 3) was collected from Longmaxi formation. Similarly, after shale sample reacted with CO<sub>2</sub> at various pressures (4 Mpa, 6 Mpa, 8 Mpa, and 16 Mpa) at 40 °C for 4 days,  $\theta_s$  for shale (LM 3) increased from 62° to 86° which was measured at 0.1 Mpa and 25 °C [56]. In contrast, after shale samples reacted with CO<sub>2</sub> at various pressures (9 Mpa, 12 Mpa, 15 Mpa, 18 Mpa, 21 Mpa and 24 Mpa) at 70 °C for 48 h,  $\theta_s$  for shales (WF, EF, MAN) increased from 69° to 84°, from 67° to 85° and decreased from 35° to 33°, respectively, which were measured at 0.1 MPa and 20 °C [29,55], as shown in Figure 7.

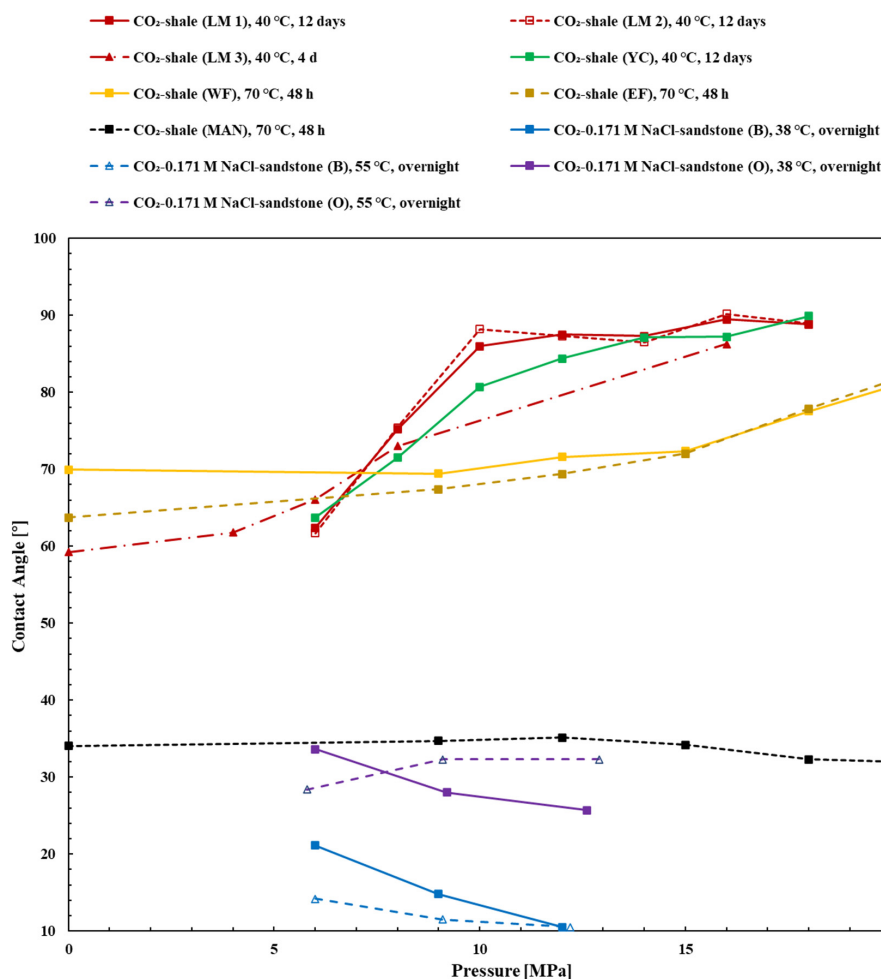


**Figure 7.** Water contact angle as a function of pressure in the H<sub>2</sub>O-rock systems after reaction with CO<sub>2</sub> [13,29,38,54,55]. 12 days: two days per pressure reaction [13,54]. The data of pressure 0 corresponds to the initial contact angle of rock.

Moreover, the effect of shale-CO<sub>2</sub> interactions on wettability was studied at various temperatures and pressures [57]. Shale samples were collected from the Qianjiang formation. After shale samples reacted with CO<sub>2</sub> at various temperatures (40 °C, 50 °C, 60 °C, 70 °C, and 80 °C at 16 MPa) and various pressures (10 MPa, 12 MPa, 14 MPa, and 16 MPa at 80 °C) for 10 days,  $\theta_5$  for shale increased from 58° to the maximum of 79°, which was measured at 0.1 MPa and 25 °C, as shown in Table 2.

**Table 2.** Changes of shale under different temperatures/pressures after shale reacted with CO<sub>2</sub> for 10 d [57].

Pressure [MPa]	Temperature [°C]	Static Contact Angle [°]	Mineral Content [%]			Chemical Groups Content	
			Quartz	Carbonate (Calcite and Dolomite)	Clay	Oxygen-Containing Groups	Hydroxyl Group
initial		58	8.5	48.0	12.1	131.9	21.4
16	40	58	9.3	47.0	11.4	76.5	21.9
16	50	68				102.3	19.5
16	60	69				113.2	18.0
16	70	75				192	13.0
16	80	73	9.5	48.9	11.8	132.7	15.8
14	80	75				167.9	14.4
12	80	79	9.7	46.7	11.2	190.3	10.4
10	80	69				100	17.4

CO<sub>2</sub> induced chemical reactions promoted mineral dissolution and generation and ion reaction, as shown in Equations (1)–(3) and (5)–(12) [13,26,45,54–56,58–61]. Shale macro-scale mineral content was varied. Carbonate [13,54,57] contents were changed and clay minerals [13,28,29,54,55,57] contents were decreased while quartz content [28,29,55] was increased. After scCO<sub>2</sub> treatment, compositional variations of surface chemical groups, hydroxyl groups [29,55] and oxygen-containing groups [57], are shown in Tables 2 and 3.

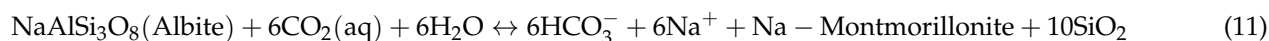
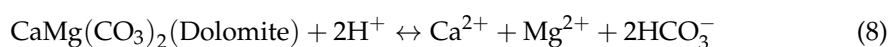
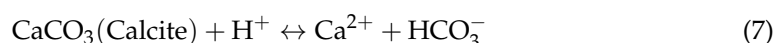


**Table 3.** Changes of shale after shale reacted with CO<sub>2</sub> at 70 °C and 18 MPa for 30 days [29,55].

Sample		Clay Content [%]	Quartz Content [%]	Surface Hydroxyl Content
WF	Before	60.9	30.2	
	After	46.3	46.7	
EF	Before	62.5	16.6	25.779
	After	56.0	23.5	21.373
MAN	Before	37.7	49.6	27.757
	After	34.3	56.5	29.814

Carbonate and clay minerals are strongly hydrophilic [4]. Hydroxyl groups can react with water to form hydrogen bonds, making the surface hydrophilic [62,63]. A decrease of carbonate, clay minerals and hydroxyl groups increase shale surface hydrophilicity. For example, after shales reacted with CO<sub>2</sub> at 70 °C and 18 MPa for 30 days, the clay content of EF decreased from 62.5% to 56% and the surface hydroxyl content decreased from 25.8 to 21.4 while  $\theta_s$  of EF increased from 65° to 100°. In addition, the clay content of MAN decreased from 37.7% to 34.3% and the surface hydroxyl content increased from 27.8 to 29.8, while  $\theta_s$  of MAN decreased from 36° to 25°.  $\theta_s$  was measured at 0.1 MPa and 20 °C, as shown in Table 3 and Figure 6. The variation of YC contact angle was more obvious than that of LM 1 and LM 2, probably due to the fact that YC contained more clay minerals [13]. The MAN's wettability decreasing with time was also because of the lower clay minerals in the MAN shale [29,55]. The clay mineral content of LM (12.9~15.3%) was lower than MAN (37.7%), but only the contact angle for MAN decreased after shales reacted with CO<sub>2</sub>. This is probably due to differences in experimental set-up and reaction conditions. For LM reactions, heating of the water bath was outside the reaction vessel while for the MAN reaction, the heating of the water vapour was inside the reaction vessel. LM reactions were at 40 °C and 8 MPa while MAN reactions were at 70 °C and 18 MPa. Moreover, the contact angles of LM and MAN had different trends after their reaction with CO<sub>2</sub>, due to different

temperature, pressure and water quantity, as shown in Figure 8 and Table 3. It should be noted that quartz is hydrophilic while shale wettability did not increase with quartz content because condensation reactions (Equation (14) [56]) weakened the hydrophilicity of quartz [57]. However, there was not a very clear relationship between oxygenated groups and shale wettability, even though the authors concluded that oxygenated groups are negatively correlated with shale wettability [57].

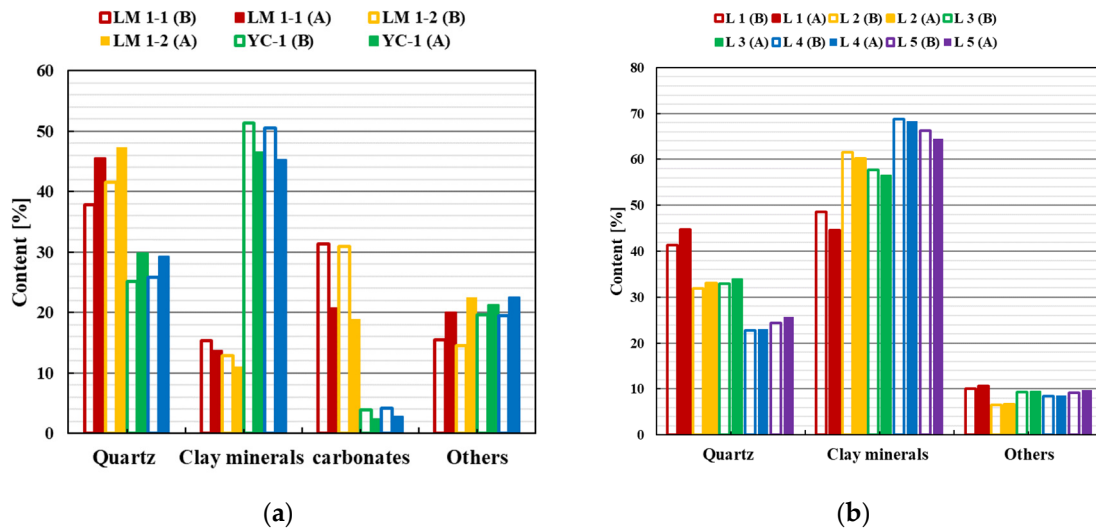


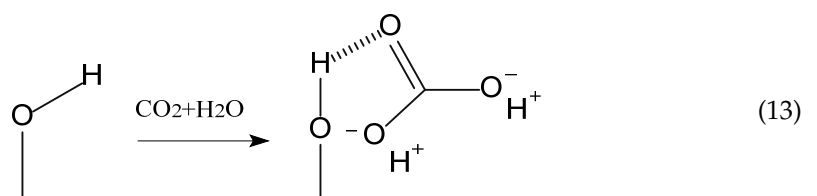
**Figure 8.** Mineral content of shale before (b) and after (a) shale reacted with CO<sub>2</sub>. (a) 10 d, 16 MPa, 40 °C [13]; (b) 6 m, 17.9 Mpa, 50 °C [28].

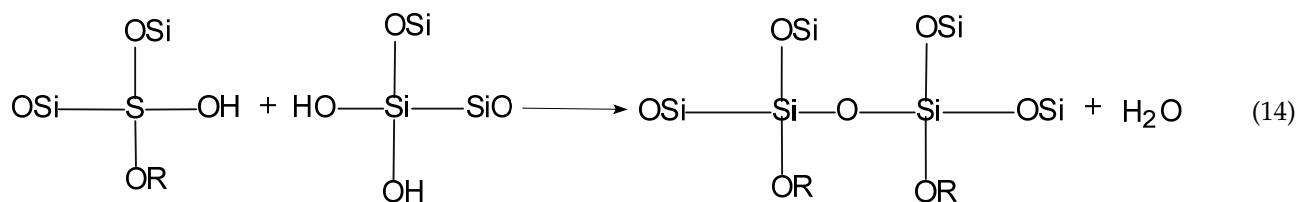
High pressure increases the solubility of CO<sub>2</sub>. The formation of carbonic acid is accelerated (Equation (13) [56]) and the above reactions are driven. For LM 3, when pressure increased from 4 Mpa to 16Mpa, the content of hydrophilic minerals decreased from 35.9 to 25.5 and ratio of the Si-OH (hydrophilic) to the Si-O-Si (hydrophobic) content decreased from 11.24 to 6.39, while  $\theta_5$  for LM 3 increased from 59° to 86°, which was measured at 0.1 MPa and 25 °C [56], as shown in Table 4. Noteworthy, the ratio of Si-OH to Si-O-Si decreased because of the polymerization reaction (Equation (14)) [56]. However, the reactions regarding the involvement of water seemed to be unreasonably interpreted because there was no water involved in the reaction except for the water inside the shale [13,54].

**Table 4.** Changes of shale (LM 3) under different pressures after shale reacted with CO<sub>2</sub> for 4 d at 40 °C [56].

Pressure [MPa]	Initial	4 MPa	6 MPa	8 MPa	16 MPa
Hydrophilic minerals components (%)	37	35.9	29.3	25.7	25.5
Ratio of the Si-OH to the Si-O-Si components		11.24	7	6.57	6.39

Hydrophilic minerals contain calcite, dolomite and clay minerals.





#### 4.2. Sandstone

Due to high permeability and porosity, sandstone is the dominant rock for CO<sub>2</sub> storage at subsurface [43,64].

After sandstones reacted with CO<sub>2</sub>-0.171 M NaCl brine at various temperatures (38 °C, 55 °C) and pressures (5.8 MPa~12.9 MPa) overnight, it showed that  $\theta_S$  for sandstones from Obernkirchener (O) and Berea (B) formation did not change with pressure and temperature in a certain pattern. Sandstones remained strongly wet [38]. For example, after sandstone (B) reacted with CO<sub>2</sub>-0.171 M NaCl at 38 °C overnight,  $\theta_S$  decreased from 21° to 11° when the pressure increased from 6 MPa to 12 MPa. Additionally, after sandstone (O) reacted with CO<sub>2</sub>-0.171 M NaCl at 13 MPa overnight,  $\theta_S$  for sandstone (O) increased from 26° to 32° when the temperature increased from 38 °C to 55 °C.  $\theta_S$  were measured at reaction conditions, as shown in Figure 7. Although pure minerals that make up sandstones changed to varying degrees,  $\theta_S$  for sandstones did not differ significantly. Two brines were prepared. Brine 1 was composed of 5 wt% NaCl, 1 wt% KCl and CO<sub>2</sub>. Brine 2 was composed of 5 wt% NaCl and 1 wt% KCl. In contrast, after the sandstone flooded by brine 1 at (10 MPa, 15 MPa) and 50 °C for 7 days, it was found that the advancing/receding angle ( $\theta_A, \theta_R$ ) in the system of CO<sub>2</sub>-brine 2-sandstone was greater and the sandstone even became CO<sub>2</sub>-wet at a higher pressure (15 MPa) at 50 °C [65], as shown in Table 5.

In principle, chemical reactions promoted sandstone dissolution and precipitation. Kaolinite precipitation was observed by SEM [65]. Sandstone wettability was altered. However, the mineral content did not change much before and after the reaction. Other mineral-related reactions were not verified in this report, as shown in Table 5 [65].

**Table 5.** Changes of sandstone under different pressures after sandstone reacted with CO<sub>2</sub> at 50 °C for 7 days [65].

Sandstone	Pressure [MPa]	Contact Angle [°]		Mineral Content [wt%]
		Advancing	Receding	
Berea	Before flooding	10	65	Quartz: 84.3 Kaolinite: 4.1 Illite: 1.9
		15	81	Albite: 4.2 Microcline: 4.1 Chorite: 1.4
	After flooding	10	74	Quartz: 58.2 Kaolinite: 3.2 Illite: 3.6
		15	89	Albite: 12.4 Muscovite: 1.6 Chorite: 5.7 Ankerite: 15.3

Table 5. Cont.

Sandstone	Pressure [MPa]	Contact Angle [°]		Mineral Content [wt%]	
		Advancing	Receding		
Bandera Gray	Before flooding	10	86	Quartz: 84.9 Kaolinite: 3.9 Illite: 1.8 Albite: 4.2 Microcline: 4.1 Chorite: 1.1	
		15	105	97	
	After flooding	10	96	90	Quartz: 58.4 Kaolinite: 3.1 Illite: 3.2 Albite: 12.2 Muscovite: 3.1 Chorite: 5.2 Ankerite: 14.8
		15	108	103	

#### 4.3. Limestone

To date, there is only one report on limestone wettability at reservoir conditions [66]. After limestone was exposed to the scCO<sub>2</sub>-1 M NaCl brine at (12 MPa, 45 ± 1 °C) for 6 months,  $\theta_S$  increased from 0° to 75°. However, an explanation for the phenomenon that limestone tended to be CO<sub>2</sub>-wet after scCO<sub>2</sub> treatment was not provided in this work.

#### 5. Research Gaps and Future Outlook

Wettability is an important parameter influencing CO<sub>2</sub> storage capacities and containment securities in saline reservoirs [4,67]. However, geo-chemical reactions occur and complicate wettability throughout the entire saline reservoir lifetime [28,29]. Current knowledge gaps are identified, and future outlook is suggested as the following:

(1) Geo-chemical reaction-induced wettability changes for quartz [36–38], calcite [36,40,44], mica [38,40,41], feldspar [38,40,44], kaolinite [38], chlorite [38], shale [13,28,29,38,54–57], sandstone [38,65] and limestone [66] have been thoroughly investigated. However, how these reactions affect the wettability of limestone, kaolinite, phlogopite, and illite need to be clarified by further studies. Moreover, other ions or components in saline aquifers can also be involved in the reactions [50], and further studies are needed to clarify the influence of these related reactions on wettability changes.

(2) The chemical reactions that may occur during CO<sub>2</sub> injections as well as sequestration have been clarified, but the specific effects of certain reactions on wettability still cannot be determined. In order to establish baselines and databases for numerical simulations, the thermodynamics and kinetics of each geo-chemical reaction should be examined rigorously and systematically as a function of duration, pressure, temperature, brine properties, rock/mineral properties, etc.

(3) The contact angle measurement process has a significant impact on the results, e.g., surface roughness [68]; surface cleaning [34,69,70]; droplet size [71–73]; static contact angle ( $\theta_R$ ) or advancing/receding contact angle ( $\theta_A$ ,  $\theta_R$ ) [34,74]. A standard contact angle measurement protocol should be developed under the consideration of surface preparation procedures, droplet/bubble generation processes and contact angle quantification aspects, etc. [17].

(4) Reaction-induced wettability changes can alter the percolation of CO<sub>2</sub>-brine, and thus affect CO<sub>2</sub> storage capacities and leakage [7], which will be an important research topic in the future.

#### 6. Conclusions

Wettability is an important parameter influencing gas storage capacities and containment securities in saline reservoirs [4–13,75–79]. Recently, many studies have been carried

out on wettability changes in CO<sub>2</sub>-liquid-mineral/rock systems affected by geo-chemical reactions, including influencing factors such as pressure, temperature, salinity and duration [13,28,29,36–38,40,41,44,54–57]. However, a critical review of the subject is still lacking. Therefore, we reviewed all available data and concluded the following:

(1) After the geo-chemical reaction with CO<sub>2</sub>, quartz, mica, kaolinite and chlorite become more CO<sub>2</sub>-wet with pressure increases but biotite becomes more water-wet with salinity increase, while calcite and feldspar's wettability do not change significantly.

(2) After rocks, including shale, sandstone, and limestone, react with CO<sub>2</sub>, their wettability changes to different degrees, which is related to the variation of their mineral content.

(3) Geo-chemical reactions change rock/mineral surface structures (e.g., surface roughness and heterogeneity) and chemistry (e.g., functional group content). As a result, mineral/rock wettability is altered.

This review systematically summarizes the effects of geochemical reactions on the alteration of wettability of the CO<sub>2</sub>-liquid-mineral/rock system and provides some guidance for long-term CO<sub>2</sub> storage in saline aquifers.

**Author Contributions:** Conceptualization, Methodology, Software, Validation, Investigation, Data curation, Writing—original draft, Writing—review and editing, T.C.; Methodology, Supervision, Writing—review and editing, L.S. and X.Z.; Conceptualization, Software, Data curation, Y.Y.; Conceptualization, Investigation, Methodology, Supervision, Writing—original draft, Writing—review and editing, Funding acquisition, H.F. and B.P. All authors have read and agreed to the published version of the manuscript.

**Funding:** This research was funded by Fundamental Research Funds for the Central Universities, grant number 00007705 and China Postdoctoral Science Foundation, 2022M720414.

**Data Availability Statement:** No new data were created or analyzed in this study.

**Acknowledgments:** B.P. acknowledges the initiative funding from the University of Science and Technology Beijing.

**Conflicts of Interest:** The authors declare no conflict of interest.

## Appendix A

**Table A1.** Contact angle measurement.

Reference	Method
Chao Qin et al., 2022 [13]	The sessile drop method
Raof Gholami et al., 2021 [28]	The sessile drop method
Ahmed Fatah et al., 2021 [29]	The sessile drop method
Prem Kumar Bikkina 2011 [36]	The sessile drop method
Yongman Kim 2012 [37]	Image processing method
Xiaozhou Zhang et al., 2020 [38]	The bubble capture method
Raheleh Farokhpoor et al., 2013 [40]	The bubble capture method
Lijie Zhang et al., 2016 [41]	The bubble capture method
Shibo Wang et al., 2013 [44]	The bubble capture method
Chao Qin et al., 2016 [54]	The sessile drop method
Ahmed Fatah et al., 2021 [55]	The sessile drop method
Yiyu Lu et al., 2021a [56]	The sessile drop method
Yiyu Lu et al., 2021b [57]	The sessile drop method
Cut Aja Fauziah et al., 2021 [65]	The sessile drop method
Shibo Wang et al., 2015 [66]	The sessile drop method

## References

1. Leung, D.Y.C.; Caramanna, G.; Maroto-Valer, M.M. An overview of current status of carbon dioxide capture and storage technologies. *Renew. Sustain. Energy Rev.* **2014**, *39*, 426–443. [[CrossRef](#)]
2. Bachu, S.; Bonijoly, D.; Bradshaw, J.; Burruss, R.; Holloway, S.; Christensen, N.P.; Mathiassen, O.M. CO<sub>2</sub> storage capacity estimation: Methodology and gaps. *Int. J. Greenh. Gas Control.* **2007**, *1*, 430–443. [[CrossRef](#)]
3. Metz, B.; Davidson, O.; De Coninck, H.; Loos, M.; Meyer, L. *IPCC Special Report on Carbon Dioxide Capture and Storage*; Cambridge University Press: Cambridge, UK, 2005.
4. Iglauer, S.; Pentland, C.H.; Busch, A. CO<sub>2</sub> wettability of seal and reservoir rocks and the implications for carbon geo-sequestration. *Water Resour. Res.* **2015**, *51*, 729–774. [[CrossRef](#)]
5. Hu, R.; Wan, J.; Kim, Y.; Tokunaga, T.K. Wettability impact on supercritical CO<sub>2</sub> capillary trapping: Pore-scale visualization and quantification. *Water Resour. Res.* **2017**, *53*, 6377–6394. [[CrossRef](#)]
6. Baban, A.; Keshavarz, A.; Amin, R.; Iglauer, S. Impact of Wettability Alteration on CO<sub>2</sub> Residual Trapping in Oil-Wet Sandstone at Reservoir Conditions Using Nuclear Magnetic Resonance. *Energy Fuels* **2022**, *36*, 13722–13731. [[CrossRef](#)]
7. Al-Khdheawi, E.A.; Vialle, S.; Barifcani, A.; Sarmadivaleh, M.; Iglauer, S. Influence of CO<sub>2</sub>-wettability on CO<sub>2</sub> migration and trapping capacity in deep saline aquifers. *Greenh. Gases Sci. Technol.* **2017**, *7*, 328–338. [[CrossRef](#)]
8. Bakhshian, S.; Hosseini, S.A. Pore-scale analysis of supercritical CO<sub>2</sub>-brine immiscible displacement under fractional-wettability conditions. *Adv. Water Resour.* **2019**, *126*, 96–107. [[CrossRef](#)]
9. Liang, Y.; Tsuji, S.; Jia, J.; Tsuji, T.; Matsuoka, T. Modeling CO<sub>2</sub>-Water-Mineral Wettability and Mineralization for Carbon Geosequestration. *Acc. Chem. Res.* **2017**, *50*, 1530–1540. [[CrossRef](#)]
10. Valle, L.M.; Rodríguez, R.; Grima, C.; Martínez, C. Effects of supercritical CO<sub>2</sub> injection on sandstone wettability and capillary trapping. *Int. J. Greenh. Gas Control.* **2018**, *78*, 341–348. [[CrossRef](#)]
11. Iglauer, S.; Al-Yaseri, A.Z.; Rezaee, R.; Lebedev, M. CO<sub>2</sub> wettability of caprocks: Implications for structural storage capacity and containment security. *Geophys. Res. Lett.* **2015**, *42*, 9279–9284. [[CrossRef](#)]
12. Iglauer, S. Optimum storage depths for structural CO<sub>2</sub> trapping. *Int. J. Greenh. Gas Control.* **2018**, *77*, 82–87. [[CrossRef](#)]
13. Qin, C.; Jiang, Y.; Zhou, J.; Zuo, S.; Chen, S.; Liu, Z.; Yin, H.; Li, Y. Influence of supercritical CO<sub>2</sub> exposure on water wettability of shale: Implications for CO<sub>2</sub> sequestration and shale gas recovery. *Energy* **2022**, *242*, 122551. [[CrossRef](#)]
14. Cassie, A.; Baxter, S. Wettability of porous surfaces. *Trans. Faraday Soc.* **1944**, *40*, 546–551. [[CrossRef](#)]
15. Iglauer, S. CO<sub>2</sub>-Water-Rock Wettability: Variability, Influencing Factors, and Implications for CO<sub>2</sub> Geostorage. *Acc. Chem. Res.* **2017**, *50*, 1134–1142. [[CrossRef](#)] [[PubMed](#)]
16. Pan, B.; Li, Y.; Zhang, M.; Wang, X.; Iglauer, S. Effect of total organic carbon (TOC) content on shale wettability at high pressure and high temperature conditions. *J. Pet. Sci. Eng.* **2020**, *193*, 107374. [[CrossRef](#)]
17. Pan, B.; Yin, X.; Iglauer, S. A review on clay wettability: From experimental investigations to molecular dynamics simulations. *Adv. Colloid Interface Sci.* **2020**, *285*, 102266. [[CrossRef](#)] [[PubMed](#)]
18. Al-Yaseri, A.Z.; Lebedev, M.; Barifcani, A.; Iglauer, S. Receding and advancing (CO<sub>2</sub> + brine + quartz) contact angles as a function of pressure, temperature, surface roughness, salt type and salinity. *J. Chem. Thermodyn.* **2016**, *93*, 416–423. [[CrossRef](#)]
19. Pan, B.; Li, Y.; Wang, H.; Jones, F.; Iglauer, S. CO<sub>2</sub> and CH<sub>4</sub> Wettabilities of Organic-Rich Shale. *Energy Fuels* **2018**, *32*, 1914–1922. [[CrossRef](#)]
20. Pan, B.; Li, Y.; Xie, L.; Wang, X.; He, Q.; Li, Y.; Hejazi, S.H.; Iglauer, S. Role of fluid density on quartz wettability. *J. Pet. Sci. Eng.* **2019**, *172*, 511–516. [[CrossRef](#)]
21. Arif, M.; Al-Yaseri, A.Z.; Barifcani, A.; Lebedev, M.; Iglauer, S. Impact of pressure and temperature on CO<sub>2</sub>-brine-mica contact angles and CO<sub>2</sub>-brine interfacial tension: Implications for carbon geo-sequestration. *J. Colloid Interface Sci.* **2016**, *462*, 208–215. [[CrossRef](#)]
22. Jia, C.; Huang, Z.; Sepehrnoori, K.; Yao, J. Modification of two-scale continuum model and numerical studies for carbonate matrix acidizing. *J. Pet. Sci. Eng.* **2021**, *197*, 107972. [[CrossRef](#)]
23. Rohmer, J.; Pluymakers, A.; Renard, F. Mechano-chemical interactions in sedimentary rocks in the context of CO<sub>2</sub> storage: Weak acid, weak effects? *Earth-Sci. Rev.* **2016**, *157*, 86–110. [[CrossRef](#)]
24. Liu, Q.; Maroto-Valer, M.M. Parameters affecting mineral trapping of CO<sub>2</sub> sequestration in brines. *Greenh. Gases Sci. Technol.* **2011**, *1*, 211–222. [[CrossRef](#)]
25. Rezaee, R.; Saeedi, A.; Iglauer, S.; Evans, B. Shale alteration after exposure to supercritical CO<sub>2</sub>. *Int. J. Greenh. Gas Control.* **2017**, *62*, 91–99. [[CrossRef](#)]
26. Mito, S.; Xue, Z.; Ohsumi, T. Case study of geochemical reactions at the Nagaoka CO<sub>2</sub> injection site, Japan. *Int. J. Greenh. Gas Control.* **2008**, *2*, 309–318. [[CrossRef](#)]
27. Jia, C.; Sepehrnoori, K.; Huang, Z.; Yao, J. Modeling and Analysis of Carbonate Matrix Acidizing Using a New Two-Scale Continuum Model. *SPE J.* **2021**, *26*, 2570–2599. [[CrossRef](#)]
28. Gholami, R.; Raza, A.; Andersen, P.; Escalona, A.; Cardozo, N.; Marín, D.; Sarmadivaleh, M. Long-term integrity of shaly seals in CO<sub>2</sub> geo-sequestration sites: An experimental study. *Int. J. Greenh. Gas Control.* **2021**, *109*, 103370. [[CrossRef](#)]
29. Fatah, A.; Bennour, Z.; Mahmud, H.B.; Gholami, R.; Hossain, M. Surface wettability alteration of shales exposed to CO<sub>2</sub>: Implication for long-term integrity of geological storage sites. *Int. J. Greenh. Gas Control.* **2021**, *110*, 103426. [[CrossRef](#)]

30. Liu, Y.; Zhu, W.; Kong, D.; Pan, B.; Yue, M. Analytical model of hydraulic fracturing horizontal well gas production capacity of a water-bearing tight sandstone reservoir considering planar heterogeneity. *Phys. Fluids* **2022**, *34*, 126603. [[CrossRef](#)]
31. Kalam, S.; Olayiwola, T.; Al-Rubaii, M.M.; Amaechi, B.I.; Jamal, M.S.; Awotunde, A.A. Carbon dioxide sequestration in underground formations: Review of experimental, modeling, and field studies. *J. Pet. Explor. Prod. Technol.* **2020**, *11*, 303–325. [[CrossRef](#)]
32. Ringrose, P.S.; Furre, A.K.; Gilfillan, S.M.V.; Krevor, S.; Landro, M.; Leslie, R.; Meckel, T.; Nazarian, B.; Zahid, A. Storage of Carbon Dioxide in Saline Aquifers: Physicochemical Processes, Key Constraints, and Scale-Up Potential. *Annu. Rev. Chem. Biomol. Eng.* **2021**, *12*, 471–494. [[CrossRef](#)] [[PubMed](#)]
33. Saraf, S.; Bera, A. A review on pore-scale modeling and CT scan technique to characterize the trapped carbon dioxide in impermeable reservoir rocks during sequestration. *Renew. Sustain. Energy Rev.* **2021**, *144*, 110986. [[CrossRef](#)]
34. Iglauer, S.; Salamah, A.; Sarmadivaleh, M.; Liu, K.; Phan, C. Contamination of silica surfaces: Impact on water–CO<sub>2</sub>–quartz and glass contact angle measurements. *Int. J. Greenh. Gas Control.* **2014**, *22*, 325–328. [[CrossRef](#)]
35. Drelich, J.W. Contact angles: From past mistakes to new developments through liquid–solid adhesion measurements. *Adv. Colloid Interface Sci.* **2019**, *267*, 1–14. [[CrossRef](#)] [[PubMed](#)]
36. Bikkina, P.K. Contact angle measurements of CO<sub>2</sub>–water–quartz/calcite systems in the perspective of carbon sequestration. *Int. J. Greenh. Gas Control.* **2011**, *5*, 1259–1271. [[CrossRef](#)]
37. Kim, Y.; Wan, J.; Kneafsey, T.J.; Tokunaga, T.K. Dewetting of silica surfaces upon reactions with supercritical CO<sub>2</sub> and brine: Pore-scale studies in micromodels. *Environ. Sci. Technol.* **2012**, *46*, 4228–4235. [[CrossRef](#)]
38. Zhang, X.; Ge, J.; Kamali, F.; Othman, F.; Wang, Y.; Le-Hussain, F. Wettability of sandstone rocks and their mineral components during CO<sub>2</sub> injection in aquifers: Implications for fines migration. *J. Nat. Gas Sci. Eng.* **2020**, *73*, 103050. [[CrossRef](#)]
39. Farokhpoor, R.; Bjørkvik, B.J.A.; Lindeberg, E.; Torsæter, O. CO<sub>2</sub> Wettability Behavior during CO<sub>2</sub> Sequestration in Saline Aquifer—An Experimental Study on Minerals Representing Sandstone and Carbonate. *Energy Procedia* **2013**, *37*, 5339–5351. [[CrossRef](#)]
40. Farokhpoor, R.; Bjørkvik, B.J.A.; Lindeberg, E.; Torsæter, O. Wettability behaviour of CO<sub>2</sub> at storage conditions. *Int. J. Greenh. Gas Control.* **2013**, *12*, 18–25. [[CrossRef](#)]
41. Zhang, L.; Kim, Y.; Jung, H.; Wan, J.; Jun, Y.-S. Effects of Salinity-Induced Chemical Reactions on Biotite Wettability Changes under Geologic CO<sub>2</sub> Sequestration Conditions. *Environ. Sci. Technol. Lett.* **2016**, *3*, 92–97. [[CrossRef](#)]
42. Chiquet, P.; Broseta, D.; Thibeau, S. Wettability alteration of caprock minerals by carbon dioxide. *Geofluids* **2007**, *7*, 112–122. [[CrossRef](#)]
43. Arif, M.; Lebedev, M.; Barifcani, A.; Iglauer, S. CO<sub>2</sub> storage in carbonates: Wettability of calcite. *Int. J. Greenh. Gas Control.* **2017**, *62*, 113–121. [[CrossRef](#)]
44. Wang, S.; Edwards, I.M.; Clarens, A.F. Wettability phenomena at the CO<sub>2</sub>-brine-mineral interface: Implications for geologic carbon sequestration. *Environ. Sci. Technol.* **2013**, *47*, 234–241. [[CrossRef](#)] [[PubMed](#)]
45. Nghiem, L.; Shrivastava, V.; Kohse, B. Modeling aqueous phase behavior and chemical reactions in compositional simulation. In Proceedings of the SPE Reservoir Simulation Symposium, The Woodlands, TX, USA, 21–23 February 2011. [[CrossRef](#)]
46. Jia, C.; Sepehrnoori, K.; Huang, Z.; Zhang, H.; Yao, J. Numerical studies and analysis on reactive flow in carbonate matrix acidizing. *J. Pet. Sci. Eng.* **2021**, *201*, 108487. [[CrossRef](#)]
47. Zhang, L.; Kim, D.; Jun, Y.S. Effects of Phosphonate Structures on Brine–Biotite Interactions under Subsurface Relevant Conditions. *ACS Earth Space Chem.* **2018**, *2*, 946–954. [[CrossRef](#)]
48. Zhang, L.; Kim, D.; Jun, Y.S. The Effects of Phosphonate-Based Scale Inhibitor on Brine–Biotite Interactions under Subsurface Conditions. *Environ. Sci. Technol.* **2018**, *52*, 6042–6049. [[CrossRef](#)]
49. Zhang, L.; Kim, D.; Kim, Y.; Wan, J.; Jun, Y.S. Effects of phosphate on biotite dissolution and secondary precipitation under conditions relevant to engineered subsurface processes. *Phys. Chem. Chem. Phys.* **2017**, *19*, 29895–29904. [[CrossRef](#)]
50. Zhang, L.; Zhu, Y.; Wu, X.; Jun, Y.S. Effects of sulfate on biotite interfacial reactions under high temperature and high CO<sub>2</sub> pressure. *Phys. Chem. Chem. Phys.* **2019**, *21*, 6381–6390. [[CrossRef](#)]
51. Duc, M.; Gaboriaud, F.; Thomas, F. Sensitivity of the acid-base properties of clays to the methods of preparation and measurement. 1. Literature review. *J. Colloid Interface Sci.* **2005**, *289*, 139–147. [[CrossRef](#)]
52. Shao, H.; Ray, J.R.; Jun, Y.S. Effects of salinity and the extent of water on supercritical CO<sub>2</sub>-induced phlogopite dissolution and secondary mineral formation. *Environ. Sci. Technol.* **2011**, *45*, 1737–1743. [[CrossRef](#)]
53. Fatah, A.; Bennour, Z.; Ben Mahmud, H.; Gholami, R.; Hossain, M.M. A Review on the Influence of CO<sub>2</sub>/Shale Interaction on Shale Properties: Implications of CCS in Shales. *Energies* **2020**, *13*, 3200. [[CrossRef](#)]
54. Qin, C.; Jiang, Y.; Luo, Y.; Xian, X.; Liu, H.; Li, Y. Effect of Supercritical Carbon Dioxide Treatment Time, Pressure, and Temperature on Shale Water Wettability. *Energy Fuels* **2016**, *31*, 493–503. [[CrossRef](#)]
55. Fatah, A.; Mahmud, H.B.; Bennour, Z.; Hossain, M.; Gholami, R. Effect of supercritical CO<sub>2</sub> treatment on physical properties and functional groups of shales. *Fuel* **2021**, *303*, 121310. [[CrossRef](#)]
56. Lu, Y.; Tian, R.; Liu, W.; Tang, J.; Li, H.; Chen, X.; Sun, X. Mechanisms of shale water wettability alteration with chemical groups after CO<sub>2</sub> injection: Implication for shale gas recovery and CO<sub>2</sub> geo-storage. *J. Nat. Gas Sci. Eng.* **2021**, *90*, 103922. [[CrossRef](#)]
57. Lu, Y.; Tian, R.; Tang, J.; Jia, Y.; Lu, Z.; Sun, X. Investigating the Mineralogical and Chemical Effects of CO<sub>2</sub> Injection on Shale Wettability at Different Reservoir Temperatures and Pressures. *Energy Fuels* **2021**, *35*, 14838–14851. [[CrossRef](#)]

58. Cheng, Y.; Zeng, M.; Lu, Z.; Du, X.; Yin, H.; Yang, L. Effects of Supercritical CO<sub>2</sub> Treatment Temperatures on Mineral Composition, Pore Structure and Functional Groups of Shale: Implications for CO<sub>2</sub> Sequestration. *Sustainability* **2020**, *12*, 3927. [[CrossRef](#)]
59. Mohamed, I.M.; He, J.; Nasr-El-Din, H.A. Carbon dioxide sequestration in sandstone aquifers: How does it affect the permeability? In Proceedings of the Carbon Management Technology Conference, Orlando, FL, USA, 7–9 February 2012. [[CrossRef](#)]
60. Pauwels, H.; Gaus, I.; le Nindre, Y.M.; Pearce, J.; Czernichowski-Lauriol, I. Chemistry of fluids from a natural analogue for a geological CO<sub>2</sub> storage site (Montmiral, France): Lessons for CO<sub>2</sub>–water–rock interaction assessment and monitoring. *Appl. Geochem.* **2007**, *22*, 2817–2833. [[CrossRef](#)]
61. Qin, C.; Jiang, Y.; Zhou, J.; Song, X.; Liu, Z.; Li, D.; Zhou, F.; Xie, Y.; Xie, C. Effect of supercritical CO<sub>2</sub> extraction on CO<sub>2</sub>/CH<sub>4</sub> competitive adsorption in Yanchang shale. *Chem. Eng. J.* **2021**, *412*, 128701. [[CrossRef](#)]
62. Zhuravlev, L. The surface chemistry of amorphous silica. Zhuravlev model. *Colloids Surf. A Physicochem. Eng. Asp.* **2000**, *173*, 1–38. [[CrossRef](#)]
63. Chen, C.; Zhang, N.; Li, W.; Song, Y. Water contact angle dependence with hydroxyl functional groups on silica surfaces under CO<sub>2</sub> sequestration conditions. *Environ. Sci. Technol.* **2015**, *49*, 14680–14687. [[CrossRef](#)]
64. Gholami, R.; Raza, A. CO<sub>2</sub> sequestration in sandstone reservoirs: How does reactive flow alter trapping mechanisms? *Fuel* **2022**, *324*, 124781. [[CrossRef](#)]
65. Fauziah, C.A.; Al-Yaseri, A.; Al-Khdheawi, E.; Jha, N.K.; Abid, H.R.; Iglauer, S.; Lagat, C.; Barifcani, A. Effect of CO<sub>2</sub> Flooding on the Wettability Evolution of Sand-Stone. *Energies* **2021**, *14*, 5542. [[CrossRef](#)]
66. Wang, S.; Tokunaga, T.K. Capillary pressure-saturation relations for supercritical CO<sub>2</sub> and brine in limestone/dolomite sands: Implications for geologic carbon sequestration in carbonate reservoirs. *Environ. Sci. Technol.* **2015**, *49*, 7208–7217. [[CrossRef](#)] [[PubMed](#)]
67. Tokunaga, T.K.; Wan, J. Capillary Pressure and Mineral Wettability Influences on Reservoir CO<sub>2</sub> Capacity. *Rev. Mineral. Geochem.* **2013**, *77*, 481–503. [[CrossRef](#)]
68. Wang, S.; Tao, Z.; Persily, S.M.; Clarens, A.F. CO<sub>2</sub> adhesion on hydrated mineral surfaces. *Environ. Sci. Technol.* **2013**, *47*, 11858–11865. [[CrossRef](#)]
69. Mahadevan, J. Comments on the paper titled “Contact angle measurements of CO<sub>2</sub>–water–quartz/calcite systems in the perspective of carbon sequestration”: A case of contamination? *Int. J. Greenh. Gas Control.* **2012**, *7*, 261–262. [[CrossRef](#)]
70. Butt, H.-J.; Graf, K.; Kappl, M. *Physics and Chemistry of Interfaces*; John Wiley & Sons: Hoboken, NJ, USA, 2023.
71. Vafaei, S.; Podowski, M.Z. Analysis of the relationship between liquid droplet size and contact angle. *Adv. Colloid Interface Sci.* **2005**, *113*, 133–146. [[CrossRef](#)]
72. Pan, B.; Clarkson, C.R.; Atwa, M.; Debuhr, C.; Ghanizadeh, A.; Birss, V.I. Wetting dynamics of nanoliter water droplets in nanoporous media. *J. Colloid Interface Sci.* **2021**, *589*, 411–423. [[CrossRef](#)]
73. Pan, B.; Clarkson, C.R.; Debuhr, C.; Younis, A.; Song, C.; Ghanizadeh, A.; Birss, V.I. Low-permeability reservoir sample wettability characterization at multiple scales: Pore-, micro- and macro-contact angles. *J. Nat. Gas Sci. Eng.* **2021**, *95*, 104229. [[CrossRef](#)]
74. Arif, M.; Abu-Khamsin, S.A.; Iglauer, S. Wettability of rock/CO<sub>2</sub>/brine and rock/oil/CO<sub>2</sub>-enriched-brine systems: Critical parametric analysis and future outlook. *Adv. Colloid Interface Sci.* **2019**, *268*, 91–113. [[CrossRef](#)]
75. Pan, B.; Yin, X.; Zhu, W.; Yang, Y.; Ju, Y.; Yuan, Y.; zhang, L.; Iglauer, S. Theoretical study of brine secondary imbibition in sandstone reservoirs: Implications for H<sub>2</sub>, CH<sub>4</sub>, and CO<sub>2</sub> geo-storage. *Int. J. Hydrogen Energy* **2022**, *47*, 18058–18066. [[CrossRef](#)]
76. Pan, B.; Yin, X.; Ju, Y.; Iglauer, S. Underground hydrogen storage: Influencing parameters and future outlook. *Adv. Colloid Interface Sci.* **2021**, *294*, 102473. [[CrossRef](#)] [[PubMed](#)]
77. Pan, B.; Yin, X.; Iglauer, S. Rock-fluid interfacial tension at subsurface conditions: Implications for H<sub>2</sub>, CO<sub>2</sub> and natural gas geo-storage. *Int. J. Hydrogen Energy* **2021**, *46*, 25578–25585. [[CrossRef](#)]
78. Pan, B.; Liu, K.; Ren, B.; Zhang, M.; Ju, Y.; Gu, J.; Zhang, X.; Clarkson, C.R.; Edlmann, K.; Zhu, W. Impacts of relative permeability hysteresis, wettability, and injection/withdrawal schemes on underground hydrogen storage in saline aquifers. *Fuel* **2023**, *333*, 126516. [[CrossRef](#)]
79. Pan, B.; Jones, F.; Huang, Z.; Yang, Y.; Li, Y.; Hejazi, S.H.; Iglauer, S. Methane (CH<sub>4</sub>) Wettability of Clay-Coated Quartz at Reservoir Conditions. *Energy Fuels* **2019**, *33*, 788–795. [[CrossRef](#)]

**Disclaimer/Publisher’s Note:** The statements, opinions and data contained in all publications are solely those of the individual author(s) and contributor(s) and not of MDPI and/or the editor(s). MDPI and/or the editor(s) disclaim responsibility for any injury to people or property resulting from any ideas, methods, instructions or products referred to in the content.